iScience

CellPress
OPEN ACCESS

Article

The atypical CDK activator RingoA/Spy1 regulates exit from quiescence in neural stem cells

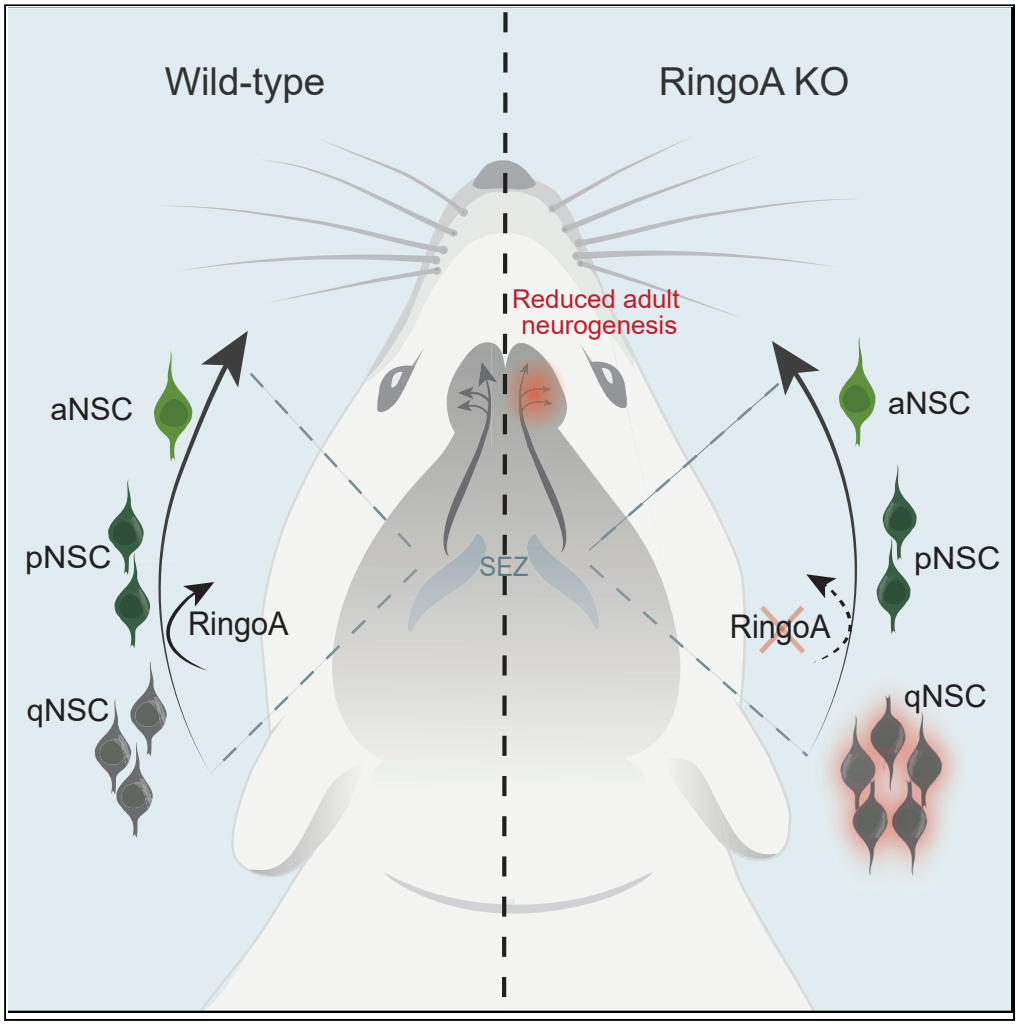

Laura Gonzalez, Ana Domingo-Muelas, Pere Duart-Abadia, ..., Jose Manuel Morante-Redolat, Isabel Fariñas, Angel R. Nebreda

isabel.farinas@uv.es (I.F.)
angel.nebreda@irbbarcelona.org (A.R.N.)

Highlights

RingoA/Spy1 regulates the exit from quiescence in adult subependymal NSCs

RingoA sets the threshold of CDK activity required for NSCs to enter the cell cycle

RingoA KO mice exhibit reduced olfactory neurogenesis

RingoA KO mice accumulate quiescent NSCs

Gonzalez et al., iScience 26, 106202
March 17, 2023
https://doi.org/10.1016/j.isci.2023.106202

iScience

CellPress
OPEN ACCESS

Article

The atypical CDK activator RingoA/Spy1 regulates exit from quiescence in neural stem cells

Laura Gonzalez,[1] Ana Domingo-Muelas,[2,3,4] Pere Duart-Abadia,[2,3,4] Marc Nuñez,[1] Petra Mikolcevic,[1] Elisabet Llonch,[1] Monica Cubillos-Rojas,[1] Begoña Cánovas,[1] Stephen M.A. Forrow,[1] Jose Manuel Morante-Redolat,[2,3,4] Isabel Fariñas,[2,3,4,*] and Angel R. Nebreda[1,5,6,*]

SUMMARY

In the adult mammalian brain, most neural stem cells (NSCs) are held in a reversible state of quiescence, which is essential to avoid NSC exhaustion and determine the appropriate neurogenesis rate. NSCs of the mouse adult subependymal niche provide neurons for olfactory circuits and can be found at different depths of quiescence, but very little is known on how their quiescence-to-activation transition is controlled. Here, we identify the atypical cyclin-dependent kinase (CDK) activator RingoA as a regulator of this process. We show that the expression of RingoA increases the levels of CDK activity and facilitates cell cycle entry of a subset of NSCs that divide slowly. Accordingly, RingoA-deficient mice exhibit reduced olfactory neurogenesis with an accumulation of quiescent NSCs. Our results indicate that RingoA plays an important role in setting the threshold of CDK activity required for adult NSCs to exit quiescence and may represent a dormancy regulator in adult mammalian tissues.

INTRODUCTION

Most mammalian tissues harbor long-lived stem cells (SCs), which balance their self-renewing proliferation with the production of differentiated progeny to compensate for physiological cell loss. Subsets of SCs can spend long periods in a quiescent state, but the molecular regulation of this state as well as the reversible transitions between dormancy and activation have started to be understood only recently. SC quiescence is not a default state in the absence of mitogens, but a highly regulated cell decision that results from the SC integration of multiple niche and systemic signals.[1–3] Furthermore, subsets of non-cycling SCs in a particular tissue can be found at varying depths of quiescence.[2] While all these cells share a transcriptional program of quiescence, some of them are more prone to engage proliferation upon mitogen stimulation. This "primed-quiescent" state has been described in adult muscle SCs, hematopoietic SCs (HSCs), and neural SCs (NSCs).[2,4–8]

In the adult mouse brain, NSCs are mainly found in the subependymal zone (SEZ) of lateral ventricle walls and in the subgranular zone (SGZ) of the dentate gyrus in the hippocampus.[3] In the SEZ, NSCs produce transit-amplifying neural progenitor cells (NPCs), which rapidly divide a few times before they progress into neuroblasts (NBs) destined to differentiate as interneurons in the olfactory bulb (OB).[9] Recent refinements of the procedure to isolate SEZ cells by fluorescence-activated cell sorting (FACS),[10–12] now allows us to collect NSCs in three states of activation: quiescent (qNSC), quiescent-primed (pNSC), and activated (aNSC).[7,13] Deep sequencing and cycling analysis of the three NSC subsets have indicated that pNSCs are molecularly quiescent but, in contrast to qNSCs, can become activated to form neurospheres *in vitro*, although they do so more slowly than aNSCs. Furthermore, molecularly defined primed-like and activated-like NSCs dividing at different rates have been detected in neurospheres growing under mitogenic stimulation.[7] The existence and interchangeability of these states suggest finely tuned mechanisms of cycling regulation the molecular details of which, however, remain unknown.

Cells enter the cell division cycle in response to growth-promoting signals during the G1 phase when a threshold of cyclin-dependent kinase (CDK) activity is reached as a result of the balance between CDK,

[1]Institute for Research in Biomedicine (IRB Barcelona), The Barcelona Institute of Science and Technology, 08028 Barcelona, Spain

[2]Departamento de Biología Celular, Biología Funcional y Antropología Física, Universidad de Valencia, 46100 Burjassot, Spain

[3]Instituto de Biotecnología y Biomedicina, Universidad de Valencia, 46100 Burjassot, Spain

[4]Centro de Investigación Biomédica en Red sobre Enfermedades Neurodegenerativas (CIBERNED), 28029 Madrid , Spain

[5]ICREA, Pg. Lluís Companys 23, 08010 Barcelona, Spain

[6]Lead contact

*Correspondence: isabel.farinas@uv.es (I.F.), angel.nebreda@irbbarcelona.org (A.R.N.)

https://doi.org/10.1016/j.isci.2023.106202

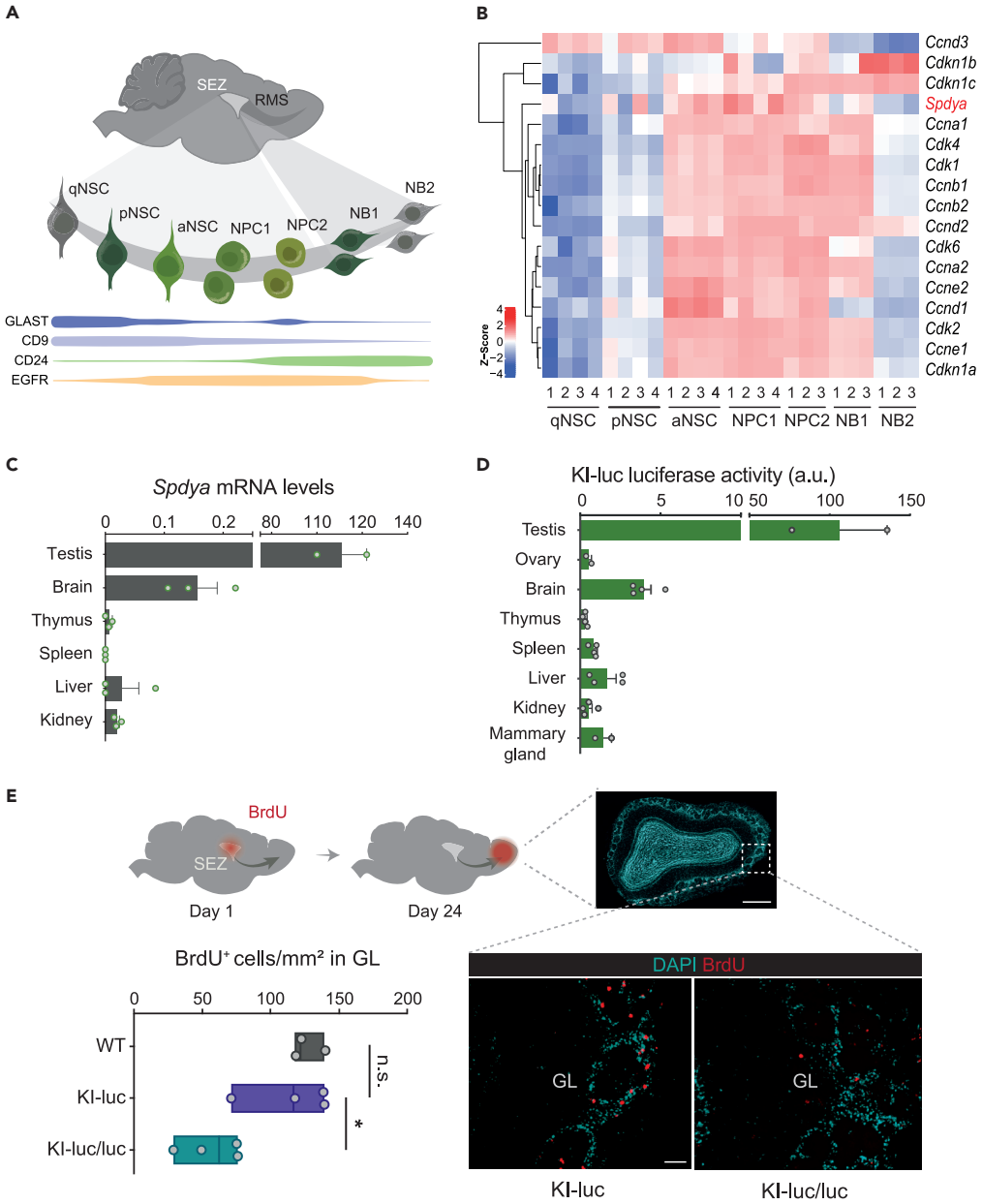

Figure 1. RingoA is expressed in proliferating subependymal cells

(A) Cells in the subependymal zone (SEZ) that are CD45$^-$ O4$^-$ CD31$^-$ Ter119$^-$, to exclude microglia, oligodendrocytes, endothelial cells and erythrocytes, were characterized by cytometry using the indicated marker. Thickness of the colored lines indicates the relative abundance of each marker along the stratified cell populations and depicts the specific combination that defines them. Neural stem cells (NSCs) are classified as quiescent (qNSC), primed (pNSC), and activated (aNSC). NPC, neural progenitor cells. NB, neuroblasts, which originate from NPCs can be proliferative (NB1) or post-mitotic (NB2).

(B) Heatmap representing the expression levels of mRNAs for cell cycle regulators including *Spdya* (encoding RingoA) in the indicated SEZ cell populations, based on transcriptomic analysis.[7] The data in the heatmap derives from an RNA-Seq experiment that included four independent cell sorting procedures of the entire SEZ neurogenic lineage with pooled cells from 3 to 4 independent mice each.

(C) *Spydya* mRNA levels were determined by RT-PCR in homogenates of different tissues. Each dot represents the tissue of a different mouse (2 males and 1 female). Bars indicate mean ± SEM (n = 2–3).

(D) Mice expressing in heterozygosis a luciferase reporter under control of the endogenous *Spdya* gene promoter (KI-luc) were injected with D-luciferin and the indicated tissues were analyzed. Each dot represents the luciferase activity in arbitrary units (a.u.) from the tissue of a mouse (2 males and 2 females). Bars indicate mean ± SEM (n = 2–4).

Figure 1. *Continued*

(E) WT, KI-luc and KI-luc/luc mice were injected with BrdU on day 1 and sacrificed on day 24 to analyze the OB. Images show OB slices with immunofluorescent detection of BrdU and DAPI as counterstain to reveal newly generated cells in the glomerular layer (GL) of KI-luc and KI-luc/luc mice. The histogram shows the quantification of $BrdU^+$ cells in 4 mice of each genotype. OB sizes do not differ between genotypes. OB cross sectional area: 3.22 ± 0.21 vs 3.11 ± 0.13 mm^2, in KI-luc and KI-luc/KI-luc respectively. GL area: 0.79 ± 0.04 vs 0.74 ± 0.03 mm^2. Floating bars (min to max) with a line at the mean. *$p < 0.05$ in an unpaired student's t-test. n.s., not significant. Scale bars: 500 μm and 30 μm (closeup). See also Figures S1 and S2.

cyclin and CDK inhibitor (CKI) levels within the cell.[14] *In vitro*, the CDK activity levels after mitosis determine whether cells start the next cell cycle or enter a transient G0-like quiescence state.[15] There is evidence that CDK6 levels increase when HSCs progress from quiescence to activation.[8] However, although CDK6 and CDK2 regulate overall proliferation and neurogenesis in the adult SEZ,[16,17] their potential contribution to NSC activation from quiescence remains unexplored.

RINGO/Speedy proteins are atypical CDK activators, which can bind to and activate CDK1 and CDK2 under conditions where CDK-cyclin complexes would be inhibited.[18–21] The mammalian family member RingoA/Spy1 (encoded by the *Spdya* gene) is essential for mouse meiosis,[22,23] and has been also proposed to participate in tumorigenesis, including a role in the proliferation of tumor-initiating $CD133^+$ glioma cells, as well as in the proliferation/differentiation of early postnatal SEZ NSCs.[24–27] However, very little is known about the functions of these atypical CDK activators in the homeostasis of adult somatic tissues where the transition between quiescent and activated SC states appears to be under tight molecular control.

Here, we show that RingoA downregulation compromises the activation of pNSCs *in vitro* and results in both increased numbers of qNSCs and reduced neurogenesis *in vivo*. Mechanistically, we provide evidence that RingoA controls the CDK2 activity levels in NSCs. These results indicate that RingoA expression sets adult NSCs closer to cell cycle entry from quiescence by increasing CDK activity in shallow-quiescent NSCs with very low CDK levels.

RESULTS

RingoA is a novel regulator of adult neurogenesis

We have recently developed a FACS method to fractionate the SEZ neurogenic lineage into different cell classes, including three subsets of NSCs,[7,13] as shown in Figure 1A and further described in STAR Methods. Our data indicated that although more than 95% of all qNSCs and pNSCs *in vivo* are in the G0 phase, pNSCs have a 3.2-fold higher probability of entering the cell cycle as determined with repetitive pulses of EdU.[7] Interrogation of our transcriptomic data[7] on the expression of cell cycle regulators revealed that qNSCs do not express detectable mRNA levels of any CDK, while pNSCs exhibit a low level that becomes very high in their fully activated counterparts. Cyclin expression followed the same dynamics but with higher variability, consistent with the dependency of their expression on the cell cycle phase. However, CKIs of the CIP/KIP family were not expressed in qNSCs or pNSCs, despite their quiescence. Expression of p21Cip1 (*Cdkn1a*) and p57Kip2 (*Cdkn1c*) started in aNSCs, and p27Kip1 (*Cdkn1b*) expression was detected even later, in NPCs (Figure 1B). The data suggested that NSCs with varying propensity to cell cycle entry may differ in CDK activity levels, including that of CDK6 as reported for HSCs.[8] Interestingly, and in contrast to other cell cycle activators, we found that the *Spdya* mRNA was increased in aNSCs and NPCs and then decreased in NBs (Figure 1B). We detected variability in *Spdya* mRNA levels, probably due to the reported oscillation of its expression during the cell cycle,[28–30] as also described for other cell cycle regulators.[31] Moreover, *Spdya* expression first appears in pNSCs (Figure 1B), which suggests that its transcription might anticipate to most other cell cycle regulators analyzed.

The *Spdya* mRNA is expressed at very low or undetectable levels in most mouse tissues with the only exception of the testis, where it is highly expressed, in agreement with its key role in meiosis.[22,23] Nevertheless, we found that the brain was the non-meiotic tissue where *Spdya* mRNA was expressed the most (Figure 1C). To further analyze *Spdya* expression, we generated a knock-in mouse line that expresses the luciferase reporter under control of the endogenous *Spdya* gene promoter (KI-luc) (Figure S1A), and confirmed that the reporter activity reproduced the observed expression of *Spdya* in different tissues (Figure 1D). Consistent with the knock-in cassette being designed to disrupt *Spdya* expression, male mice bearing the KI-luc reporter in homozygosity displayed the same atrophic testicular phenotype as the RingoA KO mice[22] (Figures S1B and S1C). Nonetheless, the brains of both KI-luc and KI-luc/luc mice exhibited an apparently

normal cytoarchitecture and were of the same size as in WT mice (Figure S2A). These results indicated that loss of RingoA does not produce any major developmental or morphological alterations in the brain. However, the *Spdya* mRNA expression that could be detected in different WT brain regions (including the SEZ) and in adult SEZ-derived NSCs, was virtually abrogated in the KI-luc/luc mice without any apparent compensatory changes in the expression of *Spdyb* (Figures S2B and S2C). Previous studies in proliferating mammalian cells have shown that the half-life of RingoA protein is less than 30 min, even shorter than the half-life of other cell cycle regulators that are known to be very unstable, such as cyclins.[29] Both the low expression level of the *Spyda* mRNA and the short half-life of the protein complicate the detection of endogenous RingoA outside the testis. Nevertheless, taking advantage of the loss of *Spydya* expression in KI-luc/luc mice, we decided to attempt the detection of the RingoA protein by comparing the intensity of WT vs. KI-luc/luc neurosphere cells using flow cytometry after staining with anti-RingoA antibodies (Figure S2D) or with anti-luciferase antibodies (Figure S2E). Although in both cases, we were able to detect a shift in the fluorescence between WT and homozygous KI cells (Figures S2D and S2E), the difference was very small and made us realize that the protein analysis in neural tissue (that expresses around 100-fold less *Spdya* mRNA than testis) was unattainable.

Despite the inability to detect RingoA protein expression in the brain and the lack of overall effects in the brain upon *Spdya* downregulation, the detection of *Spdya* mRNA expression in subependymal NSCs prompted us to characterize the role of RingoA in adult neurogenesis. We performed a 5-bromo-2′-deoxyuridine (BrdU)-based birth dating analysis to evaluate the generation of new OB neurons by injecting the mice with BrdU every 1.5 h for 9 h (seven times) and euthanizing them 24 days later (Figure 1E). With this long chase, migrating NBs that exit the cell cycle immediately after incorporating BrdU in their last S-phase retain the nucleoside and are detected as $BrdU^+$ newly generated neurons in the glomerular layer of the OB. Quantitation of periglomerular $BrdU^+$ cells revealed a clear reduction in adult neurogenesis upon *Spdya* downregulation (Figure 1E). These data indicate that RingoA is critical to sustain adult olfactory neurogenesis.

RingoA sets the threshold for quiescence exit

Our transcriptomics data in the SEZ neurogenic niche suggested that *Spdya* mRNA expression in the adult brain is elevated in proliferating cells, but downregulated in quiescent and post-mitotic cells. To confirm that RingoA expression correlated with proliferation, we generated primary neurospheres from our KI-luc mice and then cultured the cells under adhesive conditions to measure the reporter luciferase activity in media with the mitogens EGF and FGF or after mitogen withdrawal to block proliferation (Figure 2A). We detected in proliferating cells a substantial luciferase activity as a surrogate for *Spdya* expression, which was drastically reduced when cells were forced to exit the cell cycle, as demonstrated by the disappearance of the Ki67 proliferation marker (Figure 2B).

To test the possibility that RingoA could regulate NSC proliferation, we established cultures of neurospheres from $Spdya^{lox/lox}$; UBC-$CreERT2^{TG/+}$ mice that contained a ubiquitin promoter-driven inducible Cre, which allows RingoA downregulation upon treatment with 4-hydroxytamoxifen (4-OHT) (Figure 2C). Comparison of WT neurospheres with the RingoA inducible KO (iKO) counterparts obtained by incubation with 4-OHT showed no significant differences in cell cycle phase distribution, EdU labeling index or cell death rate (Figures S3A–S3C). Interestingly, RingoA iKO cells formed a significantly reduced number of neurospheres compared with WT cells, and the neurospheres were also smaller (Figures 2D and 2E). As a control, 4-OHT treatment did not affect the neurosphere formation ability of subependymal NSCs extracted from $Spdya^{+/+}$;UBC-$CreERT2^{TG/+}$ mice (Figure S3D), excluding that 4-OHT or Cre off-target effects contribute to the impaired neurosphere formation observed in RingoA iKO cells.

The reduced number and size of neurospheres, without overall changes in cell proliferation and cell death indicators, suggested a potential role of RingoA in a subset of the neurosphere initiating cells. Monitoring fluorophore dilution in neurospheres growing under strong mitogenic stimulation allows the identification of slow-dividing and fast-dividing cells that display primed-like and activated-like NSC molecular signatures, respectively. Indeed, we have previously used the fluorescent tracer DFFDA, which is diluted by half in each cell division, to study different proliferative dynamics in neurospheres. By evaluating DFFDA retention after 4 days of *in vitro* culture, we could observe the existence of fast- and slowly dividing cells in growing neurospheres, the latter retaining a pNSC molecular signature.[7] To test the possibility that RingoA loss could be differentially affecting fast and slowly dividing NSCs, we loaded single neurosphere cells obtained from $Spdya^{lox/lox}$;UBC-$CreERT2^{TG/+}$ mice with DFFDA and cultured them in neurosphere growing medium for

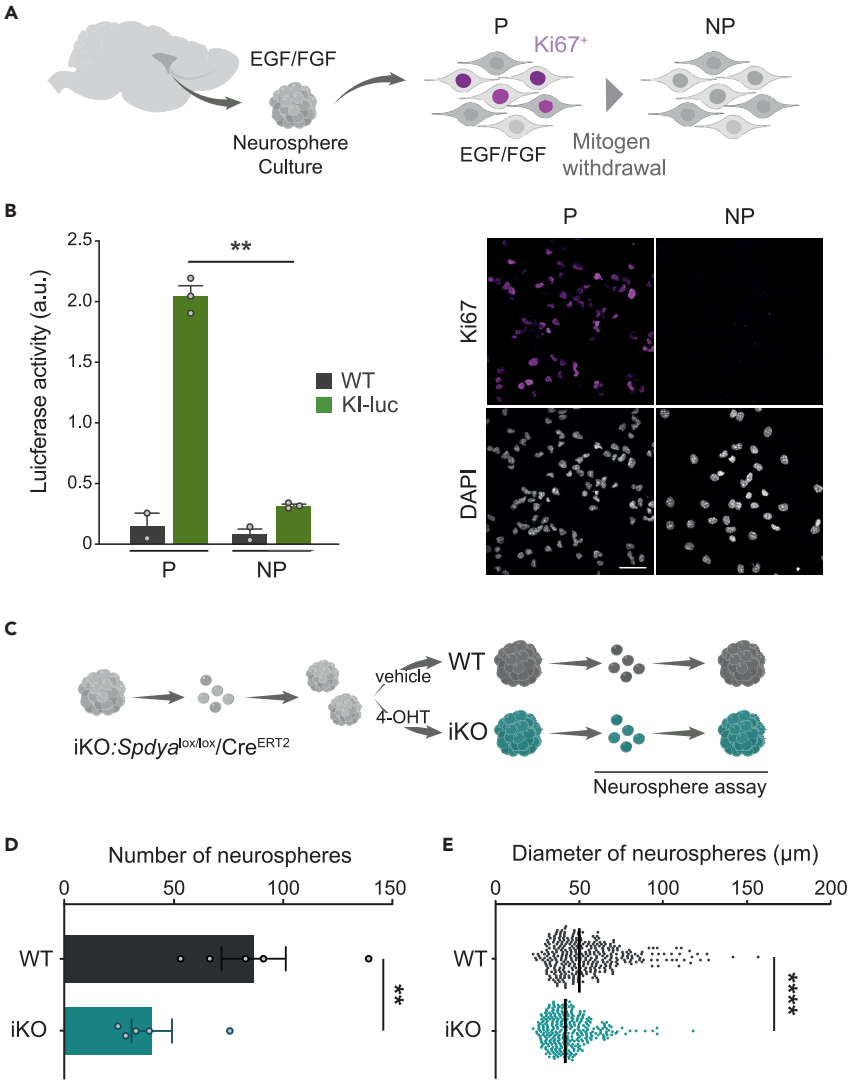

Figure 2. RingoA is important for neurogenesis in the adult brain

(A) Primary NSCs were extracted from the adult subependymal zone (SEZ) and cultured in the presence of mitogens (bFGF + EGF) to generate neurospheres, which were then dissociated and plated on laminin with the same medium containing mitogens to stimulate proliferation (P) or with EGF-free medium for 2 days followed by 1 day without any mitogens to stop proliferation (NP).

(B) The histogram (left) shows luciferase activity in arbitrary units (a.u.) in cells obtained from wild-type (WT) or KI-luc mice under the conditions indicated in (A). WT values indicate the background luminescence. Bars indicate mean ± SEM of cultures obtained from 3 different KI-luc mice. **$p < 0.01$ in a paired student's t-test. Images (right) show the immunofluorescence detection of the Ki67 proliferation marker. Cells were counterstained with DAPI. Scale bar: 30 µm.

(C) Neurospheres generated from *Spdya*$^{lox/lox}$;UBC-CreERT2$^{TG/+}$ mice were grown for 4 days and then treated with 4-OHT or with vehicle for 24 h to obtain RingoA inducible KO (iKO) and WT cells, respectively. Single cells dissociated from treated neurospheres were seeded in growth medium to generate new neurospheres and after 7 days in culture their number and size were quantified.

(D) Number of neurospheres formed by RingoA iKO neurosphere-initiating cells compared to those formed by WT cells. Bars indicate mean ± SEM of data obtained from 5 independent cultures. **$p < 0.01$ in a paired student's t-test.

(E) Diameter of the neurospheres formed by RingoA iKO neurosphere-initiating cells compared to those formed by WT cells. Data represent all the neurospheres in each condition from 5 independent cultures. The mean is indicated by a line, ****$p < 0.0001$ in a paired student's t-test. See also Figure S3.

4 days. Then, *Spdya* deletion was induced with 4-OHT and 24 h later fluorophore-retaining (DFFDA^{high}) and nonretaining (DFFDA^{low}) cells were sorted by FACS and plated in EGF and bFGF-containing medium to assess cell doublet formation (Figure 3A). We scored a similar number of DFFDA^{low} fast-dividing cells in the two genotypes. However, fewer DFFDA^{high} cells entered the cell cycle in the absence of RingoA in comparison with WT cells, an effect that was not due to the 4-OHT treatment, suggesting a requirement for RingoA in DFFDA^{high} cells to start dividing (Figures 3A and 3B). Considering the higher self-renewing capacity of slow-dividing cells,[7] it seems likely that loss of RingoA sets a higher threshold for the activation of these cells, which can explain the reduced secondary neurosphere yield observed in RingoA iKO cultures. These results identify RingoA as a regulator of slow-dividing primed-like NSCs.

We next decided to test whether the mechanism underlying the RingoA effect on the NSC activation threshold was related to its capacity to allosterically activate CDK1 and CDK2.[30] We took advantage of the live-cell sensor CSII-EF-DHB-mVenus that has been reported to monitor CDK2 activity in asynchronously dividing cultures at the single-cell level.[15] This reporter includes the C-terminal domain of the human DNA helicase B, which can be phosphorylated by CDK2, fused to the yellow fluorescent protein mVenus. The unphosphorylated reporter is primarily located in the nucleus, but its phosphorylation during the G1/S transition results in the reporter being exported to the cytoplasm.[15,33] Neurosphere cells were infected with a lentivirus containing the reporter and plated as single cells for image analysis. Quantification of the mVenus fluorescence ratio in cytoplasm versus nucleus allowed us to identify cells with either active or inactive CDK2 (Figure 3C). We found that RingoA downregulation resulted in a significantly lower percentage of cells with active CDK2 and a concomitant increase in the percentage of cells with inactive CDK2 (Figure 3D). These results support a role for RingoA in controlling CDK2 activity in NSCs, which in turn correlates with NSC division rate.

The requirement for RingoA to sustain normal neurogenesis *in vivo* and its involvement in the regulation of the threshold for activation of slowly dividing NSCs prompted us to evaluate the effect of the loss of RingoA in the SEZ neurogenic lineage *in vivo*. As mentioned above, our transcriptomic analysis detected higher levels of *Spdya* mRNA expression in aNSC and NPC populations (Figure 4A). Consistent with the idea that RingoA facilitates NSC proliferation and neurogenesis, EdU-labeled cells detected 1 h after EdU injection into mice indicated that overall cell proliferation *in vivo* was reduced in the SEZ of KI-luc/luc mice compared to WT mice (Figure 4B). This overall reduction in EdU incorporation observed in KI-luc/luc mice could be the result of either fewer proliferative cells in the lineage or a lower cell cycling rate in some populations. Therefore, we next set out to study the SEZ neurogenic lineage cell composition, and the proliferative activity of the different cell fractions in the absence of RingoA. To do so, we used our recently developed methodology to quantify different SEZ cell populations and their proliferation by FACS.[7,13] Cytometry-based phenotyping of SEZ subpopulations in KI-luc/luc mice revealed a clear increase in the qNSC population accompanied by a decrease in neuroblasts at the end of the lineage (Figure 4C, left). Furthermore, the EdU-labeling rate in each individual population was not affected by RingoA downregulation (Figure 4C, right). The results indicate that RingoA does not play a major role in cell cycling, but it is necessary for the activation of a dormant phenotype, in line with our *in vitro* analysis. Altogether, our data support that RingoA is an important regulator of adult neurogenesis through its involvement in the timely activation of quiescent NSCs.

DISCUSSION

The use of newly developed techniques for the separation of SEZ cell subpopulations by FACS offers an opportunity to understand cell population dynamics and cell cycle regulation *in vivo*. This type of analysis together with deep sequencing approaches have unveiled the existence of different levels of quiescence in SC populations, although their regulation is not understood.[2,14] Our results identify the atypical CDK activator RingoA as an important regulator of cell cycle entry in slow-cycling NSCs, providing insights into the regulation of SC quiescence. We also show that genetic deletion of RingoA results in reduced neurogenesis *in vivo*. Phenotyping of the SEZ lineage at the single cell level indicates that the effect of RingoA in the rate of adult neurogenesis is linked to its role in facilitating the entry of quiescent NSCs into the cell cycle. Taken together, our results identify a novel role for noncanonical CDK activators in the regulation of shallow SC quiescence.

RingoA has been reported to regulate the proliferation of tumor-initiating CD133^{+} human glioma cells, and the proliferation/differentiation of NSCs obtained from the SEZ of mouse pups.[27] This work also reported the detection of the RingoA protein in human brain tumors, a situation far from what we observe in mouse brains and normal NSCs. The differences may indicate species divergences or that *Spdya* upregulation

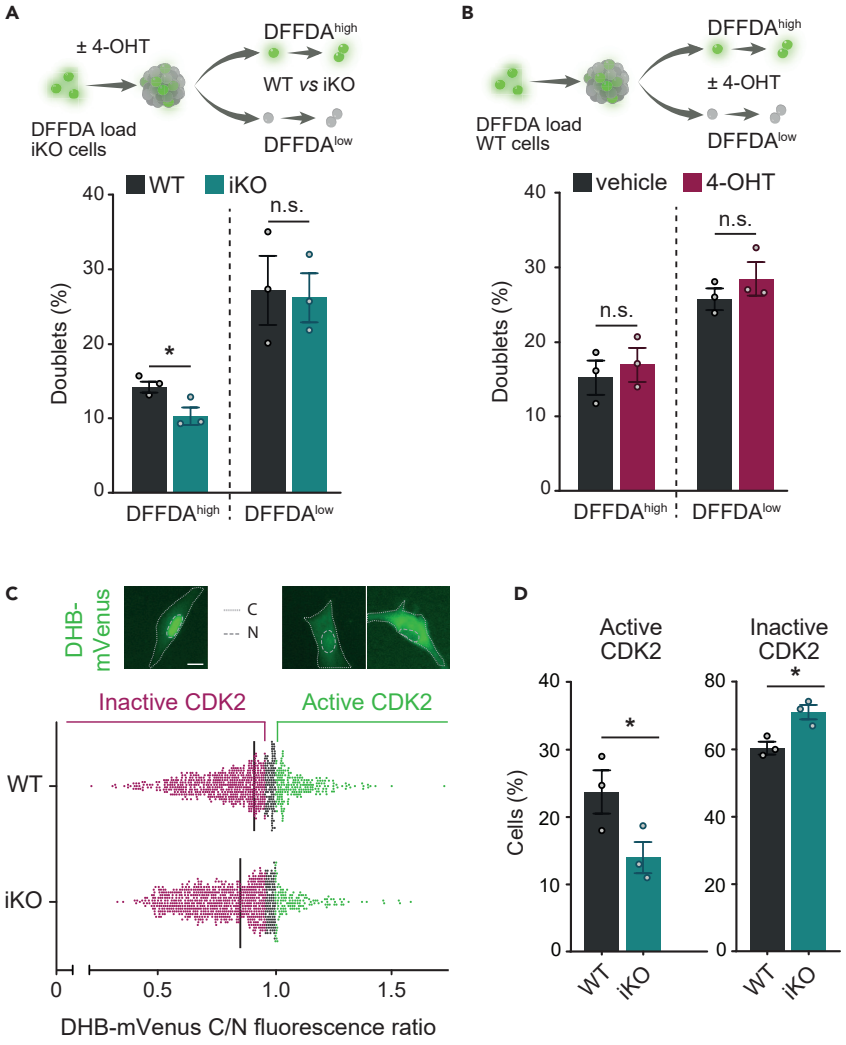

Figure 3. RingoA regulates neurosphere fitness and CDK2 activity

(A) Neurospheres obtained from *Spdya*$^{lox/lox}$;UBC-CreERT2$^{TG/+}$ mice were loaded with 2 μg/mL of DFFDA, cultured for 4 days and then treated with 4-OHT to generate the RingoA inducible KO (iKO) or with vehicle for 24 h. After dissociation, DFFDA-high and DFFDA-low cells from WT and RingoA iKO neurospheres were sorted and plated, and 24 h later cell doublets were counted. The graph shows the percentage of doublets in each population of WT and RingoA iKO cultures. Bars indicate mean ± SEM of data obtained from 3 independent cultures. *p < 0.05 in an unpaired student's t-test. n.s., not significant.

(B) Neurospheres obtained from WT mice were loaded with 2 μg/mL of DFFDA and cultured for 4 days. After neurosphere dissociation, DFFDA^{high} and DFFDA^{low} cells were sorted and plated in the presence of 4-OHT or vehicle, and 24 h later cell doublets were counted. The graph shows the percentage of doublets in each treatment. Bars indicate mean ± SEM of data obtained from 3 independent cultures. n.s., not significant in an unpaired student's t-test.

(C) Neurospheres obtained from *Spdya*$^{lox/lox}$;UBC-CreERT2$^{TG/+}$ mice were infected with lentivirus expressing the reporter CSII-EF-DHB-mVenus to measure CDK2 activity. After sorting, neurospheres were treated with 4-OHT (RingoA iKO) or with vehicle (WT) for 48 h, and then dissociated and cultured as single cells for image analysis. The mVenus fluorescence is detected mostly in the nucleus of cells with low CDK2 activity, but it is stronger in the cytoplasm of cells with increased CDK2 activity. Nuclei were identified by staining with DRAQ5. The graph shows CDK2 activity *per* cell, which was calculated as the cytoplasm versus nucleus (C/N) fluorescence intensity ratio. The C/N ratio of the reporter remains very low in G0 (around 0.6) and starts to rise during G1 reaching values >1 in S and G2/M phases.[32] In our analysis, cells with C/N ratio >1 were considered to have active CDK2, and with <0.95 were considered to have CDK2 inactive as reported.[32] Scale bar: 10 μm.

(D) Percentages of WT and RingoA iKO cells with active (C/N > 1) and inactive (C/N < 0.95) CDK2. Bars indicate mean ± SEM of data from 3 independent cultures. *p < 0.05 in an unpaired student's *t* test.

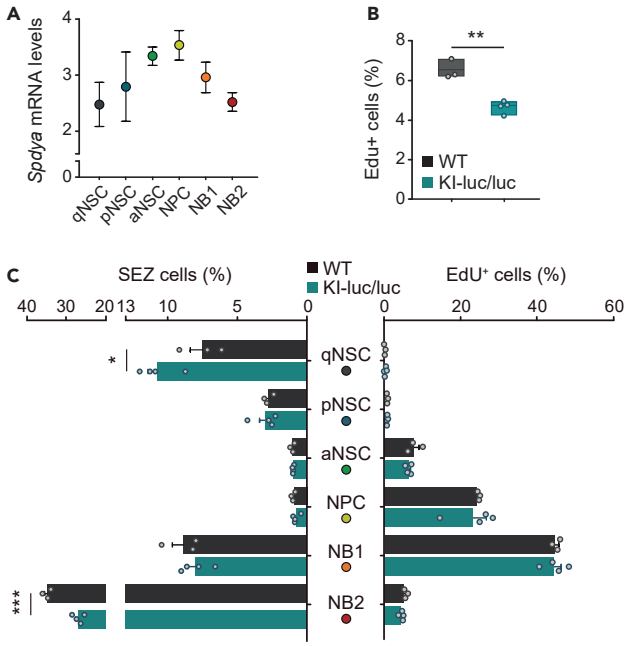

Figure 4. The number of quiescent NSCs increases in the intact SEZ of RingoA deficient mice

(A) Expression of the *Spdya* mRNA (encoding RingoA) in the indicated subependymal zone (SEZ) cell populations isolated by FACS. Data obtained from the RNA sequencing described in.[7] Neural stem cells (NSCs) that are quiescent (qNSC), primed (pNSC), or activated (aNSC). NPC, neural progenitor cell. NB, neuroblast.

(B) Wild-type (WT) and KI-luc/luc mice were injected with EdU 1 h before euthanasia. The SEZ was dissociated and the percentage of EdU-incorporating cells was assessed by cytometry. Bars indicate mean ± SEM of data from 3 WT to 4 KI-luc/luc mice, respectively. **$p < 0.01$ in an unpaired student's t-test.

(C) The SEZ was isolated from WT and KI-luc/luc mice (n = 4 independent animals *per* genotype) 1 h after an EdU injection, and the proportions of each SEZ neurogenic population (left) as well as the EdU-labeling rate *per* cell population (right) were determined by cytometry. The data indicate that qNSC are more numerous at the expense of derived NBs, and that RingoA deficiency does not affect the cycling rate of proliferating SEZ cells. Bars indicate mean ± SEM. *$p < 0.05$ and ***$p < 0.001$ in an unpaired student's t-test. All samples without asterisks are not significant.

confers a proliferative advantage to brain tumor initiating cells, as could be expected from our own data. RingoA levels are extremely low in the mouse neurogenic lineage, but play a critical role in the capacity of shallow-quiescent NSCs to engage cycling. A previous study using NSCs isolated from the neonatal SEZ also indicated extremely low levels of *Spdya* expression, but functional effects *in vitro* both in preventing NSC differentiation and in stimulating proliferation.[27] The mouse SEZ achieves its adult cytoarchitecture around 6 weeks after birth[9] when the different NSC states and dynamics can be recognized. Indeed, intermediate quiescent states have only been molecularly defined in the adult niche allowing to place RingoA in the regulation of the quiescence-activation balance. Our data highlights that elucidating relevant functions of very low levels of a critical protein in distinct cell populations requires high resolution approaches.

Our expression data indicate that quiescent NSCs may have limited and variable CDK activities. Thus, the dependence of NSCs on RingoA for CDK activation probably relies on the specific properties of CDK-RingoA compared to CDK-cyclin complexes. Namely, RINGO-activated CDKs do not require T-loop phosphorylation and are less sensitive to CKIs.[20,21,34] These peculiarities could be especially relevant in the context of NSCs, which are able to proliferate despite expressing high levels of p21Cip1 and p57Kip1 mRNAs.[35–38] Our data suggest that RingoA may play a key regulatory role in setting the threshold of activation in SCs with very low levels of CDK. It remains to be investigated whether RingoA could also regulate cell cycle entry in SCs from other tissues.

The observation that unlike cyclins, RingoA starts to be expressed in pNSCs, together with its importance in triggering the proliferation of slowly dividing NSCs, suggest some parallelism with the mechanism for cell cycle entry in *Xenopus* oocytes. G2 arrested oocytes provide an unfavorable biochemical environment for

canonical CDK activation by cyclins, but expression of RINGO/Speedy suffices to break the cell-cycle arrest by inducing the activation of monomeric CDK1. This small level of RINGO/Speedy-induced CDK activity triggers a positive feedback loop, which eventually leads the oocyte to enter M phase.[34,39] Similarly, the expression of RingoA in shallow quiescent NSCs, in which most cell cycle inducers are absent, might allow pNSCs to activate a threshold of CDK activity, which through positive feedback loops could lead to enhanced expression of cyclins and downregulation of inhibitory mechanisms, further increasing CDK activity and allowing cell cycle entry. Consistent with this idea, we show that RingoA downregulation results in reduced CDK activity and qNSCs accumulation *in vivo*, supporting a defect in NSC quiescence exit.

Our results indicate a clear function of RingoA in adult neurogenesis. The apparent lack of effects on embryonic neurogenesis may be related to the presence of CDK4 activity in fetal neural progenitors, which can functionally complement for the absence of CDK2.[17,40] Thus, RingoA might have a higher impact in a context where CDK2 has a role that cannot be functionally complemented by other CDKs. Alternatively, SC quiescence in adult tissues required for the lifelong maintenance of SC pools and tissue homeostasis[2] may rely on additional regulatory layers as the one described here.

Limitations of the study

The main caveat of the present study is that the expression of RingoA protein in NSCs appears to be extremely low. Loss-of-function data obtained with genetic mouse models support the implication of RingoA in quiescence exit of adult NSCs, but experiments correlating RingoA levels with cell function are precluded by its low levels of expression. We have tested various home-made and commercial RingoA antibodies, which all recognize the overexpressed RingoA but failed to detect the endogenous protein in brain sections, and the detected levels in isolated NSCs are very low. This is a technical limitation that for the time being prevents further mechanistic studies on the role of CDK2-RingoA in NSC quiescence exit.

STAR★METHODS

Detailed methods are provided in the online version of this paper and include the following:

- KEY RESOURCES TABLE
- RESOURCE AVAILABILITY
  - Lead contact
  - Materials availability
  - Data and code availability
- EXPERIMENTAL MODEL AND SAMPLE DETAILS
- METHOD DETAILS
  - SEZ analysis by flow cytometry
  - BrdU-labeling and immunohistochemistry
  - RNA extraction and gene expression analysis
  - Bioluminescence and fluorescence imaging
  - Neurosphere cultures
  - Intracellular protein detection by flow cytometry
  - Proliferation and cell death analyses
  - CDK2 reporter analysis in neurospheres
- QUANTIFICATION AND STATISTICAL ANALYSIS
  - Quantitative analysis
  - Statistical analysis

SUPPLEMENTAL INFORMATION

Supplemental information can be found online at https://doi.org/10.1016/j.isci.2023.106202.

ACKNOWLEDGMENTS

We acknowledge the technical support of the mouse mutant, advanced digital microscopy, and histopathology facilities of IRB Barcelona, the Cytometry facility of the Universidad de Barcelona, and the Servicio Central de Soporte a la Investigación Experimental of the Universidad de Valencia (SCSIE-UVEG). We thank Dr Tobias Meyer (Stanford University Medical Center) for generously providing the CDK2 reporter, Dr Eric Brown (University of Pennsylvania) for UBC-CreERT2 mice, and Camille Stephan Otto-Attolini, Nevenka

Radic and Nerea González (IRB Barcelona) for helping with statistical analyses, image analyses, and neurosphere cultures, respectively. This work was supported by Ministerio de Ciencia e Innovación (MICINN) grants BFU2004–03566, CSD2010-0045 (CONSOLIDER), and BFU2013-46377 to A.R.N.; PID2020-117937GB-I00, CB06/05/0086 (CIBERNED), and RD16/0011/0017 (RETIC Tercel) to I.F.; and the Generalitat Valenciana grant Prometeo 2017/030 to I.F. L.G. and P.D.-A. were recipients of MICINN's FPI predoctoral contracts, and A.D.-M. was the recipient of an FPU predoctoral contract from Ministerio de Educación, Cultura y Deporte (MECD). Collaborative work between I.F. and A.R.N. groups was part of the iDIFFER network (RED2018-102723-T) funded by MICINN. IRB Barcelona is the recipient of institutional funding from MICINN through the Centers of Excellence Severo Ochoa award and from the Centres de Recerca de Catalunya (CERCA) Program of the Catalan Government.

AUTHOR CONTRIBUTIONS

L.G., A.D.-M., P.D.-A., M.N., P.M., E.L., M.C.-R., B.C., and J.M.M.-R. performed the experiments and analyzed the data. S.M.A.F. was involved in the design and generation of *Spdya*$^{KI\text{-}luc}$ mice. L.G., J.M.M.-R., I.F., and A.R.N. were involved in the design of the experiments, data analysis, and writing of the article. I.F. and A.R.N. supervised the study and secured funding.

DECLARATION OF INTERESTS

The authors declare no competing interests.

Received: August 31, 2022
Revised: December 21, 2022
Accepted: February 10, 2023
Published: February 14, 2023

REFERENCES

1. Cheung, T.H., and Rando, T.A. (2013). Molecular regulation of stem cell quiescence. Nat. Rev. Mol. Cell Biol. *14*, 329–340. https://doi.org/10.1038/nrm3591.

2. van Velthoven, C.T.J., and Rando, T.A. (2019). Stem cell quiescence: dynamism, restraint, and cellular idling. Cell Stem Cell *24*, 213–225. https://doi.org/10.1016/j.stem.2019.01.001.

3. Urbán, N., Blomfield, I.M., and Guillemot, F. (2019). Quiescence of adult mammalian neural stem cells: a highly regulated rest. Neuron *104*, 834–848. https://doi.org/10.1016/j.neuron.2019.09.026.

4. Rodgers, J.T., King, K.Y., Brett, J.O., Cromie, M.J., Charville, G.W., Maguire, K.K., Brunson, C., Mastey, N., Liu, L., Tsai, C.R., et al. (2014). MTORC1 controls the adaptive transition of quiescent stem cells from G 0 to GAlert. Nature *510*, 393–396. https://doi.org/10.1038/nature13255.

5. Rodgers, J.T., Schroeder, M.D., Ma, C., and Rando, T.A. (2017). HGFA is an injury-regulated systemic factor that induces the transition of stem cells into GAlert. Cell Rep. *19*, 479–486. https://doi.org/10.1016/j.celrep.2017.03.066.

6. Llorens-Bobadilla, E., Zhao, S., Baser, A., Saiz-Castro, G., Zwadlo, K., and Martin-Villalba, A. (2015). Single-cell transcriptomics reveals a population of dormant neural stem cells that become activated upon brain injury. Cell Stem Cell *17*, 329–340. https://doi.org/10.1016/j.stem.2015.07.002.

7. Belenguer, G., Duart-Abadia, P., Jordán-Pla, A., Domingo-Muelas, A., Blasco-Chamarro, L., Ferrón, S.R., Morante-Redolat, J.M., and Fariñas, I. (2021). Adult neural stem cells are alerted by systemic inflammation through TNF-alpha receptor signaling. Cell Stem Cell *28*, 285–299.e9. https://doi.org/10.1016/j.stem.2020.10.016.

8. Laurenti, E., Frelin, C., Xie, S., Ferrari, R., Dunant, C.F., Zandi, S., Neumann, A., Plumb, I., Doulatov, S., Chen, J., et al. (2015). CDK6 levels regulate quiescence exit in human hematopoietic stem cells. Cell Stem Cell *16*, 302–313. https://doi.org/10.1016/j.stem.2015.01.017.

9. Obernier, K., and Alvarez-Buylla, A. (2019). Neural stem cells: origin, heterogeneity and regulation in the adult mammalian brain. Development *146*, dev156059. https://doi.org/10.1242/dev.156059.

10. Beckervordersandforth, R., Tripathi, P., Ninkovic, J., Bayam, E., Lepier, A., Stempfhuber, B., Kirchhoff, F., Hirrlinger, J., Haslinger, A., Lie, D.C., et al. (2010). In vivo fate mapping and expression analysis reveals molecular hallmarks of prospectively isolated adult neural stem cells. Cell Stem Cell *7*, 744–758. https://doi.org/10.1016/j.stem.2010.11.017.

11. Codega, P., Silva-Vargas, V., Paul, A., Maldonado-Soto, A.R., DeLeo, A.M., Pastrana, E., and Doetsch, F. (2014). Prospective identification and purification of quiescent adult neural stem cells from their in vivo niche. Neuron *82*, 545–559. https://doi.org/10.1016/j.neuron.2014.02.039.

12. Mich, J.K., Signer, R.A., Nakada, D., Pineda, A., Burgess, R.J., Vue, T.Y., Johnson, J.E., and Morrison, S.J. (2014). Prospective identification of functionally distinct stem cells and neurosphere-initiating cells in adult mouse forebrain. Elife *3*, 026699. https://doi.org/10.7554/eLife.02669.

13. Belenguer, G., Duart-Abadia, P., Domingo-Muelas, A., Morante-Redolat, J.M., and Fariñas, I. (2021). Cell population analysis of the adult murine subependymal neurogenic lineage by flow cytometry. STAR Protoc. *2*, 100425. https://doi.org/10.1016/j.xpro.2021.100425.

14. Urbán, N., and Cheung, T.H. (2021). Stem cell quiescence: the challenging path to activation. Development *148*, dev165084. https://doi.org/10.1242/dev.165084.

15. Spencer, S.L., Cappell, S.D., Tsai, F.C., Overton, K.W., Wang, C.L., and Meyer, T. (2013). The proliferation-quiescence decision is controlled by a bifurcation in CDK2 activity at mitotic exit. Cell *155*, 369–383. https://doi.org/10.1016/j.cell.2013.08.062.

16. Beukelaers, P., Vandenbosch, R., Caron, N., Nguyen, L., Belachew, S., Moonen, G., Kiyokawa, H., Barbacid, M., Santamaria, D., and Malgrange, B. (2011). Cdk6-dependent regulation of G1 length controls adult neurogenesis. Stem Cell. *29*, 713–724. https://doi.org/10.1002/stem.616.

17. Jablonska, B., Aguirre, A., Vandenbosch, R., Belachew, S., Berthet, C., Kaldis, P., and Gallo, V. (2007). Cdk2 is critical for proliferation and self-renewal of neural progenitor cells in the adult subventricular

zone. J. Cell Biol. *179*, 1231–1245. https://doi.org/10.1083/jcb.200702031.

18. Ferby, I., Blazquez, M., Palmer, A., Eritja, R., and Nebreda, A.R. (1999). A novel p34(cdc2)-binding and activating protein that is necessary and sufficient to trigger G2/M progression in Xenopus oocytes. Genes Dev. *13*, 2177–2189. https://doi.org/10.1101/gad.13.16.2177.

19. Lenormand, J.L., Dellinger, R.W., Knudsen, K.E., Subramani, S., and Donoghue, D.J. (1999). Speedy: a novel cell cycle regulator of the G2/M transition. EMBO J. *18*, 1869–1877. https://doi.org/10.1093/emboj/18.7.1869.

20. Karaiskou, A., Perez, L.H., Ferby, I., Ozon, R., Jessus, C., and Nebreda, A.R. (2001). Differential regulation of Cdc2 and Cdk2 by RINGO and cyclins. J. Biol. Chem. *276*, 36028–36034. https://doi.org/10.1074/jbc.M104722200.

21. McGrath, D.A., Fifield, B.A., Marceau, A.H., Tripathi, S., Porter, L.A., and Rubin, S.M. (2017). Structural basis of divergent cyclin-dependent kinase activation by Spy1/RINGO proteins. EMBO J. *36*, 2251–2262. https://doi.org/10.15252/embj.201796905.

22. Mikolcevic, P., Isoda, M., Shibuya, H., Del Barco Barrantes, I., Igea, A., Suja, J.A., Shackleton, S., Watanabe, Y., and Nebreda, A.R. (2016). Essential role of the Cdk2 activator RingoA in meiotic telomere tethering to the nuclear envelope. Nat. Commun. *7*, 11084. https://doi.org/10.1038/ncomms11084.

23. Tu, Z., Bayazit, M.B., Liu, H., Zhang, J., Busayavalasa, K., Risal, S., Shao, J., Satyanarayana, A., Coppola, V., Tessarollo, L., et al. (2017). Speedy A–Cdk2 binding mediates initial telomere–nuclear envelope attachment during meiotic prophase I independent of Cdk2 activation. Proc. Natl. Acad. Sci. USA *114*, 592–597. https://doi.org/10.1073/pnas.1618465114.

24. Al Sorkhy, M., Ferraiuolo, R.M., Jalili, E., Malysa, A., Fratiloiu, A.R., Sloane, B.F., and Porter, L.A. (2012). The cyclin-like protein Spy1/RINGO promotes mammary transformation and is elevated in human breast cancer. BMC Cancer *12*, 45. https://doi.org/10.1186/1471-2407-12-45.

25. Ferraiuolo, R.M., Tubman, J., Sinha, I., Hamm, C., and Porter, L.A. (2017). The cyclin-like protein, SPY1, regulates the ERa and ERK1/2 pathways promoting tamoxifen resistance. Oncotarget *8*, 23337–23352. https://doi.org/10.18632/oncotarget.15578.

26. Fifield, B.A., Qemo, I., Kirou, E., Cardiff, R.D., and Porter, L.A. (2019). The atypical cyclin-like protein Spy1 overrides p53-mediated tumour suppression and promotes susceptibility to breast tumourigenesis. Breast Cancer Res. *21*, 140. https://doi.org/10.1186/s13058-019-1211-3.

27. Lubanska, D., Market-Velker, B.A., deCarvalho, A.C., Mikkelsen, T., FidalgodaSilva, E., and Porter, L.A. (2014). The cyclin-like protein spy1 regulates growth and division characteristics of the CD133+ population in human glioma. Cancer Cell *25*, 64–76. https://doi.org/10.1016/j.ccr.2013.12.006.

28. Porter, L.A., Dellinger, R.W., Tynan, J.A., Barnes, E.A., Kong, M., Lenormand, J.L., and Donoghue, D.J. (2002). Human Speedy: a novel cell cycle regulator that enhances proliferation through activation of Cdk2. J. Cell Biol. *157*, 357–366. https://doi.org/10.1083/jcb.200109045.

29. Dinarina, A., Santamaria, P.G., and Nebreda, A.R. (2009). Cell cycle regulation of the mammalian CDK activator RINGO/Speedy A. FEBS Lett. *583*, 2772–2778. https://doi.org/10.1016/j.febslet.2009.07.028.

30. Gonzalez, L., and Nebreda, A.R. (2020). RINGO/Speedy proteins, a family of non-canonical activators of CDK1 and CDK2. Semin. Cell Dev. Biol. *107*, 21–27. https://doi.org/10.1016/j.semcdb.2020.03.010.

31. Martínez-Alonso, D., and Malumbres, M. (2020). Mammalian cell cycle cyclins. Semin. Cell Dev. Biol. *107*, 28–35. https://doi.org/10.1016/j.semcdb.2020.03.009.

32. Daigh, L.H., Liu, C., Chung, M., Cimprich, K.A., and Meyer, T. (2018). Stochastic endogenous replication stress causes ATR-triggered fluctuations in CDK2 activity that dynamically adjust global DNA synthesis rates. Cell Syst. *7*, 17–27.e3. https://doi.org/10.1016/j.cels.2018.05.011.

33. Overton, K.W., Spencer, S.L., Noderer, W.L., Meyer, T., and Wang, C.L. (2014). Basal p21 controls population heterogeneity in cycling and quiescent cell cycle states. Proc. Natl. Acad. Sci. USA *111*, E4386–E4393. https://doi.org/10.1073/pnas.1409797111.

34. Gutierrez, G.J., Vögtlin, A., Castro, A., Ferby, I., Salvagiotto, G., Ronai, Z., Lorca, T., and Nebreda, A.R. (2006). Meiotic regulation of the CDK activator RINGO/Speedy by ubiquitin-proteasome-mediated processing and degradation. Nat. Cell Biol. *8*, 1084–1094. https://doi.org/10.1038/ncb1472.

35. Kippin, T.E., Martens, D.J., and Van Der Kooy, D. (2005). P21 loss compromises the relative quiescence of forebrain stem cell proliferation leading to exhaustion of their proliferation capacity. Genes Dev. *19*, 756–767. https://doi.org/10.1101/gad.1272305.

36. Porlan, E., Morante-Redolat, J.M., Marqués-Torrejón, M.Á., Andreu-Agulló, C., Carneiro, C., Gómez-Ibarlucea, E., Soto, A., Vidal, A., Ferrón, S.R., and Fariñas, I. (2013). Transcriptional repression of Bmp2 by p21 Waf1/Cip1 links quiescence to neural stem cell maintenance. Nat. Neurosci. *16*, 1567–1575. https://doi.org/10.1038/nn.3545.

37. Marqués-Torrejón, M.Á., Porlan, E., Banito, A., Gómez-Ibarlucea, E., Lopez-Contreras, A.J., Fernández-Capetillo, O., Vidal, A., Gil, J., Torres, J., and Fariñas, I. (2013). Cyclin-dependent kinase inhibitor p21 controls adult neural stem cell expansion by regulating Sox2 gene expression. Cell Stem Cell *12*, 88–100. https://doi.org/10.1016/j.stem.2012.12.001.

38. Furutachi, S., Matsumoto, A., Nakayama, K.I., and Gotoh, Y. (2013). P57 controls adult neural stem cell quiescence and modulates the pace of lifelong neurogenesis. EMBO J. *32*, 970–981. https://doi.org/10.1038/emboj.2013.50.

39. Ruiz, E.J., Hunt, T., and Nebreda, A.R. (2008). Meiotic inactivation of Xenopus Myt1 by CDK/XRINGO, but not CDK/Cyclin, via site-specific phosphorylation. Mol. Cell *32*, 210–220. https://doi.org/10.1016/j.molcel.2008.08.029.

40. Lim, S., and Kaldis, P. (2012). Loss of Cdk2 and Cdk4 induces a switch from proliferation to differentiation in neural stem cells. Stem Cell. *30*, 1509–1520. https://doi.org/10.1002/stem.1114.

41. Ruzankina, Y., Pinzon-Guzman, C., Asare, A., Ong, T., Pontano, L., Cotsarelis, G., Zediak, V.P., Velez, M., Bhandoola, A., and Brown, E.J. (2007). Deletion of the developmentally essential gene ATR in adult mice leads to age-related phenotypes and stem cell loss. Cell Stem Cell *1*, 113–126. https://doi.org/10.1016/j.stem.2007.03.002.

42. Schneider, C.A., Rasband, W.S., and Eliceiri, K.W. (2012). NIH Image to ImageJ: 25 years of image analysis. Nat. Methods *9*, 671–675. https://doi.org/10.1038/nmeth.2089.

43. Belenguer, G., Domingo-Muelas, A., Ferrón, S.R., Morante-Redolat, J.M., and Fariñas, I. (2016). Isolation, culture and analysis of adult subependymal neural stem cells. Differentiation. *91*, 28–41. https://doi.org/10.1016/j.diff.2016.01.005.

STAR★METHODS

KEY RESOURCES TABLE

REAGENT or RESOURCE	SOURCE	IDENTIFIER
Antibodies		
Mouse monoclonal anti-BrdU (Bromodeoxyuridine)	Dako	Cat#M0744; RRID: AB_10013660
CD45-BUV395 (clone, rat 30-F11)	BD Biosciences	Cat#565967; RRID: AB_2739420
O4-AF405 (clone, mouse O4)	R&D Systems	Cat#FAB1326V
CD31-BUV395 (clone, rat 390)	BD Biosciences	Cat#740239; RRID: AB_2739986
Ter119-BUV395 (clone, rat TER-119)	BD Biosciences	Cat#563827; RRID: AB_2738438
GLAST-PE (clone, mouse ACSA-1)	Miltenyi	Cat#130-095-821; RRID: AB_10829184
CD24-BB700 (clone, rat M1/69)	BD Biosciences	Cat#746122; RRID: AB_2743489
CD9-Vio770 (clone, rat MZ3)	Miltenyi	Cat#130-102-384; RRID: AB_2659590
Cy3 anti-mouse	Jackson ImmunoResearch	Cat#715-165-151; RRID: AB_2315777
Rabbit anti-RingoA	Mikolcevic et al., 2016[22]	Antiserum #1870
Rabbit monoclonal anti-Firefly luciferase	Abcam	Catab185923; RRID:AB_2819349
Donkey anti-rabbit AF647	Abcam	Catab150075
Chemicals, peptides, and recombinant proteins		
Epidermal growth factor (EGF)-Alexa Fluor™ 488	Molecular Probes	Cat#E13345
Streptavidin-BV421	BD Biosciences	Cat# 563259; RRID: AB_2869475
Dulbecco's PBS (DPBS)	Sigma	Cat#D1408
Trypsin inhibitor	Sigma	Cat#T6522; CAS: 9035-81-8
5-Ethynyl-2′- deoxyuridine (EdU)	Life Technologies	Cat#E10187; CAS: 61135-33-9
4′, 6-diamidino-2′-phenylindole, dihydrochloride (DAPI)	Sigma	Cat#D9542; CAS: 28718-90-3
BD Cytofix/Cytoperm™	BD Biosciences	Cat#554722
5-Bromo-2′-deoxyuridine (BrdU)	Sigma	Cat#B5002; CAS: 59-14-3
Accutase	Sigma	Cat# A6964
B27	Life Technologies	Cat#17504044
CellTrace™ Oregon Green 488 Carboxy-DFFDA-SE	Thermo Fisher	Cat#C34555
DRAQ5TM Fluorescent Probe	ThermoFisher	Cat# 62251
EGF	Preprotech	Cat# AF10015
bFGF	Preprotech	Cat# 100-18B
Heparin	Stem Cell	Cat# 07980
Matrigel	Corning	Cat# 356231
Neurobasal medium	Life Technologies	Cat# 2110349
L-Glutamine	Gibco	Cat#25030024; CAS: 56-85-9
4-Hydrotamoxifen (4-OHT)	Sigma	Cat#7176; CAS: 68392-35-8
DNAse treatment	ThermoFisher	Cat# 12185010
Polybrene	Sigma	Cat# H9268
PureLink™ RNA mini kit	Thermo Fisher	Cat# 12183020
RNAsin	Promega	Cat# N211

(*Continued on next page*)

Continued

REAGENT or RESOURCE	SOURCE	IDENTIFIER
Super-Script IV reverse transcriptase	Invitrogen	Cat# 18090010
TRIzol reagent	ThermoFisher	Cat# 15596026
Critical commercial assays		
Luciferase Assay System	Promega	Cat# E1501
Click-iT™ EdU Alexa Fluor™ 647 Flow Cytometry Assay Kit	ThermoFisher	Cat# C10419
Experimental models: Cell lines		
HEK293-T cells	ATCC	CRL-3216
Experimental models: Organisms/strains		
Mouse: UBC-CreERT2	Ruzankina et al., 2007[41]	N/A
Mouse: *Spdya*$^{lox/lox}$	Mikolcevic et al., 2016[22]	N/A
Mouse: *Spdya*$^{KI\text{-}luc/luc}$	This paper	N/A
Oligonucleotides		
See Table S1	This paper	N/A
Recombinant DNA		
DHB-mVenus-containing plasmid	Spencer et al., 2013[15]	N/A
Software and algorithms		
ImageJ	Schneider et al., 2012[42]	https://imagej.nih.gov/ij/
FlowJo™10	BD Biosciences	https://www.flowjo.com
GraphPad Prism	GraphPad	https://www.graphpad.com
Other		
BD LSRFortessa™ Flow Cytometer	BD Biosciences	https://www.bdbiosciences.com/
Gallios Flow Cytometer	Beckman Coulter	https://www.beckman.es/resources/videos/products/gallios-overview
FACSAria III	BD Biosciences	https://www.bdbiosciences.com/
ScanR High-Content Screening Station for Life Science	Olympus	https://www.olympus-lifescience.com/es/microscopes/inverted/scanr/

RESOURCE AVAILABILITY

Lead contact

Further information and requests for resources and reagents should be directed to and will be fulfilled by the lead contact, Angel R. Nebreda (angel.nebreda@irbbarcelona.org).

Materials availability

The mouse lines used in this study are available to academic groups upon signing of an MTA.

Data and code availability

- All data are available from the lead contact upon request.
- This paper does not report original code.
- Any additional information required to reanalyze the data reported in this paper is available from the lead contact upon request.

EXPERIMENTAL MODEL AND SAMPLE DETAILS

RingoA conditional KO mice (*Spdya*$^{lox/lox}$) were generated by flanking exon 3 of the *Spdya* gene encoding RingoA with *loxP* sequences as described.[22] To generate RingoA inducible KO (iKO) mice, *Spdya*$^{lox/lox}$ animals were crossed with mice carrying UBC-CreERT2.[41]

The RingoA luciferase reporter (*Spdya*$^{KI\text{-}luc}$) was generated by the IRB Barcelona's Mouse Mutant facility. The targeting vector was prepared from an H2B-venus-luciferase gene targeting cassette (a generous gift from Dr Barry Rosen, Welcome Trust Sanger Center) by exchanging the H2B-Venus for TurboFP635 (Katushka), thereby creating a cassette containing the Katushka cDNA, a 2A sequence and the luciferase cDNA followed by an SV40 polyA sequence. The whole cassette was flanked by L1 and L2 gateway sites, which allowed it to be placed between the *Spdya* homologous arms in a 3-way gateway reaction. This created a gene-targeting vector that inserted an in-frame dual reporter cassette into intron 2–3 of the RingoA-encoding gene, immediately downstream of the first coding exon. The vector was transfected into ES cells to generate mice carrying the knock-in allele.

Mice (*Mus musculus*, C57BL/6J) were housed in the specific pathogen-free (SPF) mouse facility of the Barcelona Science Park (PCB, Barcelona) or in the mouse facility of the University of Valencia. Experiments were performed following the European Union, national and institutional guidelines, and experimental protocols were approved by the Animal Care and Use Committees of the PCB (CEEA-PCB) or the University of Valencia. All mice were maintained under a standard 12 h light/12 h dark cycle at 23°C, with free access to food and water. Male and female animals were used between the ages of 2 and 4 months.

METHOD DETAILS

SEZ analysis by flow cytometry

SEZ lineage analysis was performed as described.[13] Homogenized samples were incubated at 4°C for 30 min in 100 μL blocking buffer (HBSS without calcium and magnesium, 10 mM HEPES, 2 mM EDTA, 0.1% glucose, 0.5% BSA) containing EGF-A488 (Molecular Probes, E13345; 1:300), and primary antibodies CD24-BB700 (BD Biosciences, 746122; 1:300), GLAST-PE (Miltenyi, 130-095-821; 1:100) and CD9-APC-Vio770 (Miltenyi, 130-102-384; 1:20), after negative immunomagnetic selection of neurogenic lineage-positive cells with antibodies to CD45-BUV395 (BD Biosciences, 565967; 1:200), O4-A405 (R&D Systems, FAB1326V; 1:100), CD31-BUV395 (BD Biosciences, 740239; 1:100), and Ter119-BUV395 (BD Biosciences, 563827; 1:200).

Briefly, SEZ dissociates are gated by size and cellular complexity to discard cell debris, myelin, dead cells as well as ependymal cells and neurons and then CD45$^+$ (immune cells, mainly microglia), CD31$^+$ (endothelial), TER119$^+$ (erythrocytes) and O4$^+$ (oligodendrocytes) cells are negatively immune selected. The remaining lineage-negative (Lin$^-$) cells are subsequently labeled using fluorescent antibodies to GLAST and CD24 and fluorescent EGF to label the EGFR, a receptor associated with all proliferative populations of the neurogenic lineage.[11] The GLAST$^-$CD24^{high} fraction are NBs, which can be subsequently subdivided into EGFR$^+$ and EGFR$^{low/-}$ pools of proliferating early NBs and non-proliferating late NBs, respectively. GLAST$^-$CD24$^{-/low}$EGFR$^+$ and GLAST$^+$CD24^{high}EGFR$^+$ cells correspond to NPCs (1 and 2) that appear to behave similarly at the functional level.[7] Within the GLAST$^+$CD24$^{-/low}$ fraction, cells with low levels of CD9 are considered mature non-neurogenic astrocytes whereas CD9^{high} NSCs can be classified into different states by GLAST intensity and fluorescent EGF binding: GLAST^{high}CD24$^{-/low}$CD9^{high}EGFR$^{-/low}$ qNSCs and GLAST^{low}CD24$^{-/low}$CD9^{high}EGFR$^{-/low}$ pNSCs are quiescent whereas GLAST^{low}CD24$^{-/low}$CD9^{high}EGFR$^+$ aNSCs are proliferative.[7,13]

For cell proliferation analysis, 4 months-old mice were intraperitoneally injected with a single dose of EdU (50 mg/kg) 1 h before euthanasia and the SEZ homogenates were processed for flow cytometry as explained above.[13] Stained cells were fixed with Cytofix/Cytoperm (BD) and EdU staining was developed with the Click-iT Plus EdU Alexa Fluor 647 Flow Cytometry Assay kit (Thermo Fisher, C10419) following the manufacturer's instructions. All samples were analyzed in an LSR-Fortessa cytometer (Becton Dickinson) with 350, 488, 561 and 640 nm lasers.

BrdU-labeling and immunohistochemistry

To evaluate the generation of new OB neurons from SEZ, 3 months-old mice were given a total of 7 injections of 50 mg/kg BrdU with 1.5 h gaps, and 24 days later were anesthetized with 150 μL of 100 mg/mL ketamine and 200 μL of 1 mg/mL medetomidine, and transcardially perfused with 20 mL saline solution, followed by 75–100 mL 4% paraformaldehyde (PFA) in 0.1 M phosphate buffer pH 7.4. Coronal 40-μm-thick free-floating sections were generated with a vibratome, incubated in 2 N HCl for 20–30 min at 37 °C and neutralized in 0.1 M sodium borate (pH 8.5) before the incubation with BrdU antibodies (Dako, M0744; 1:250). Images were taken with an LSM780 (Zeiss) confocal microscope. For brain area measurements,

some coronal sections containing the SEZ from the different genotypes were Nissl stained using 0.1% cresyl violet. For the testis anatomical analysis, the organs were extracted after perfusion and fixed with 4% PFA at 4°C overnight, embedded in paraffin, sectioned into 4 μm-thick sections, and stained with hematoxylin and eosin. Samples were scanned with a NanoZoomer 2.0-HT slide scanner (Hamamatsu Photonics).

RNA extraction and gene expression analysis

Cells were washed with PBS (PBS) and resuspended in 500 μL TRIzol reagent (Invitrogen), and tissue samples were homogenized using a Percellys instrument. Chloroform (100 μL) was added and tubes were centrifuged 15,000 g at RT for 10 min. From the two liquid phases generated, the fraction with less density was transferred into new tubes. After adding 200 μL of 70% ethanol, RNA was extracted using the PureLink RNA mini kit (Thermo Fisher, 12183020) and DNAse treatment was performed using on-column DNase treatment following manufacturer's instructions (ThermoFisher, 12185010). cDNA was obtained from 500 ng to 4 μg of purified RNA using random primers, RNAsin (Promega, N211) and Super-Script IV reverse transcriptase (Invitrogen, 18090010) following the manufacturer's instructions. RT-qPCR was performed using SYBR green in a BioRad C1000 Thermal Cycler. Samples were analyzed in triplicates and normalized to GAPDH and β-Actin reference genes. Analysis was done using the ΔCt method. Primers: *Spdya*- Fw. TTCTTGTGGATGGACTGCTG/Rv. TTGCCAGATGTAATGGGTTG; β-*Actin*- Fw. GGCACCACACCTTCTAC AATG/Rv. GTGGTGGTGAAGCTGTAGCC; *GAPDH*- Fw. CTTCACCACCATGGAGGAGGC/Rv. GGCATG GACTGTGGTCATGAG (Table S1).

To analyze the neural expression of *Spdya* and *Spydb*, we dissected specific brain areas from WT and KI-luc/luc mice or used SEZ derived neurospheres from already stablished primary cultures that were pelleted after 4–5 days growing. Total RNA was extracted with the Maxwell16 LEV simplyRNA Tissue Kit (Promega, AS1280) in a Maxwell16 instrument (Promega, AS2000). Total RNA was also obtained from WT testis following the same method to be used as reference standard curve. The cDNAs were synthetized from 1 μg of the purified RNA with the PrimeScript RT reagent kit (Takara, RR037A) in the presence of both 50 pmol random hexamers and 25 pmol oligo-dT primer following the manufacturer's instructions. The relative amount of each gene was quantified in triplicates by RT-qPCR with TB Green Premix Ex Taq (Tli RNase H Plus) (Takara, RR420A) adding ROX dye in a Step One Plus instrument (Applied Biosystems) using a 10-fold serial dilution standard curve made with WT testis cDNA. Primers: *Spdya*(exon1-exon3)- Fw. CTGAGGTAGATCGCTGAGGC/Rv. AGCAGCAGTCCATCCACAAG; *Spdya*(exon3-exon4)- Fw. TCTTGTG GATGGACTGCTGC/Rv. GCTCTCTTGAAATAAACAAAGGTCA; *Spdyb*(exon2-exon4)- Fw. GTCTTCACCA AGCTGCTCG/Rv. GTACTGCCAGGAGAAGAGCC (Table S1). The reaction conditions were optimized for each primer pair in order to ensure a close to 100% amplification (standard curve slope = −3.32).

Bioluminescence and fluorescence imaging

Mice were anesthetized and injected retro-orbitally with D-luciferin (75 mg/kg). Immediately after injection, animals were sacrificed and the organs were placed in an IVIS Spectrum CT chamber for bioluminescence imaging. Data were recorded using Living Image software (Xenogen). For detection of luciferase activity in neural cells, single cells were seeded in neurosphere growth medium in plates which had been pre-treated for 2 h at 37°C with 1:100 Matrigel dilution (BD 356231) and then washed. To stop proliferation, cells were cultured for two days in control media [Neurobasal medium (Life Technologies, 2110349),1% penicillin/streptomycin, 1% L-glutamine and 2% B27 (Life Technologies, 17504044)] supplemented with 10 ng/mL bFGF (Preprotech, 100–18B), followed by 24 h with control media supplemented with 2% FBS. 100,000 cells were lysed and processed with the Luciferase Assay System (Promega, E1501) following manufacturer instructions.

Neurosphere cultures

Primary NSC cultures were established and subcultured as previously described.[43] Briefly, SEZ from 3 months-old mice were dissected and chopped into small pieces. Tissues were then incubated with an enzymatic solution at 37°C to allow tissue digestion. The reaction was stopped by washing with medium without growth factors and the cells were dissociated by adding 1 mL of medium and pipetting up and down through a p1000 micropipette tip. Cells were seeded in neurosphere growth medium [Neurobasal medium (Life Technologies, 2110349), supplemented with 2% B27 supplement (Life Technologies, 17504044), 20 ng/mL EGF (Preprotech, AF10015), 10 ng/mL bFGF (Preprotech, 100–18B), 2 μg/mL Heparin (Stem Cell, 07980), 1% penicillin/streptomycin and 1% L-glutamine] for 7–10 days at 37°C in a 5% CO_2 humidified incubator. For neurosphere subculture, spheres were disaggregated using Accutase (Sigma,

A6964) and seeded at 10,000 viable cells/cm^2 density. For freezing, the cell suspension was centrifuged and resuspended in freezing medium (90% neurosphere growth full medium, 10% DMSO) and transferred into cryo-tubes. Cryo-tubes were placed in Mr Frosty Freezing Containers (ThermoFisher) at −80 °C for 24 h and then transferred to liquid nitrogen for long-term storage. To induce *Spdya* deletion, cells were treated for 2 days with 75 μM 4-OHT from a 1 mM stock in 100% ethanol. Gene deletion was confirmed by qPCR using *Spdya* exon3 primers in combination with *Spdya* exon6 as reference. Primers: *Spdya*-exon3 Fw. TGCTTTGGGGCCAGTGAGATGA/Rv. GGCTGCTAAAGCGCATGCTCCA; *Spdya*-exon6 Fw. GGACCTAG TGCCACACCACACCAGT/Rv. GGTATGAGGAGGGTCACCTG (Table S1).

Intracellular protein detection by flow cytometry

In order to assess RingoA protein levels by flow cytometry, neurospheres from WT or KI luc/luc mice were dissociated with Accutase (Sigma, A6964). Individual cells were then washed with PBS (300 xg, 10 min) and fixed with either Cytofix/CytopermTM solution (BD Bioscience, 554722) or methanol (20 min at 4°C). Then, cells were washed with FACS buffer containing saponin and incubated with 100 μL of the primary antibodies, either homemade rabbit anti-RingoA antiserum #1870[22] at 1:5 or rabbit monoclonal anti-Firefly luciferase antibody (Abcam, ab185923) at 1:50, in FACS buffer at 4°C for 30 min. After another washing step, cells were incubated with 100 μL of a donkey anti-rabbit AF647 secondary antibody (Abcam, ab150075) at 1:400 (30 min at 4°C). Immunostained samples were centrifuged (300 xg, 10 min) and resuspended in 0.5 mL of FACS buffer for analysis in an LSR-Fortessa cytometer (Becton Dickinson) with 350, 405, 488, 561 and 640 nm lasers. APC background signal was stablished by staining cells only with secondary antibody.

Proliferation and cell death analyses

For cell cycle analysis, neurospheres were disaggregated and singlets were harvested, fixed in 70% ice-cold ethanol, and stored at −20 °C for at least 4 h. Cells were then washed and resuspended in PBS supplemented with 25 μg/mL propidium iodide and 0.1 mg/mL RNAseA (PI staining solution) and incubated for 20 min at RT. EdU incorporation was analyzed with Click-iT EdU Alexa Fluor 647 Flow Cytometry Assay Kit (ThermoFisher, C10419) following the manufacturer's instructions. For cell death analysis, DAPI was added to non-fixed cells. Samples were analyzed in a Gallios Flow Cytometer (Beckman Coulter).

For fluorophore dilution analyses,[7] neurosphere cultures were individualized and loaded with 2 μg/mL of CellTrace Oregon Green 488 Carboxy-DFFDA SE (Thermo Fisher, C34555), then cultured for 4 days in neurosphere growth medium. Grown neurospheres were treated with 75 μM 4-OHT for 24 h and dissociated for FACS separation. DFFDA^{high} (10% brightest) and DFFDA^{low} (40% dimmest) cells were sorted in a BD FACSAria III using a 100-μm nozzle at 20 psi. 500 cells were sorted into 200 μL of neurosphere growth medium[43] and doublet formation was evaluated after 24 h in a phase-contrast inverted microscope.

CDK2 reporter analysis in neurospheres

Lentiviruses were generated in HEK293-T cells by co-transfecting DHB-mVenus-containing plasmid[15] with VSV-G and Δ89 packaging DNAs. The following day, cells were washed and cultured in neurosphere growth full medium to collect the supernatant at 24 and 48 h. Neurospheres were disaggregated and 1 × 10^6 cells were incubated for 3 h with lentiviral supernatant diluted 1:1 in fresh neurosphere growth medium and supplemented with 4 μg/mL polybrene (Sigma, H9268). After 4 days, cells positive for DHB-mVenus were sorted and expanded for two weeks.

To delete *Spdya*, cells were treated for 2 days with 75 μM 4-OHT. Live cells were sorted and plated at 4,000 cells/well in 96-well plates (Falcon 353219), which had been pre-treated for 2 h at 37°C with 1:100 Matrigel dilution (BD 356231) and then washed. After 20 h, cells were fixed in 4% PFA for 20 min at RT. Cell nuclei were stained with DRAQ5TM Fluorescent Probe (ThermoFisher, 62251) following the manufacturer's instructions.

QUANTIFICATION AND STATISTICAL ANALYSIS

Quantitative analysis

The relative number of BrdU$^+$ cells in the glomerular layer of the OB was determined with the ImageJ multipoint tool. Brain dimensions were determined using ImageJ software.

For CDK2 reporter quantification, neurosphere cells were stained with DRAQ5TM Fluorescent Probe and whole-well scans were obtained with a scanR High-Content Screening Station for Life Science (Olympus). For each cell, the nucleus and a cytoplasm ring were segmented based on DRAQ5TM nuclear staining and mean intensity was quantified. The ratio of cytoplasm and nuclear intensity values (C/N) was calculated to assess CDK activity levels.

For cell proliferation and cell death analysis, around 10,000 cells were acquired on a Gallios Flow Cytometer (Beckman Coulter) and cell cycle distribution was analyzed and quantified with the FlowJo software.

Statistical analysis

All statistical tests were performed using the GraphPad Prism Software, version 5.00 forWindows (http://www.graphpad.com). Analyses of significant differences between means were assessed using the unpaired or paired two-tailed Student's *t* test or one-way ANOVA with Tukey post-hoc test when appropriate. When comparisons were carried out with relative values (normalized values and percentages), data were first normalized by using a log or arcsine transformation, respectively.